Environ. Res. Lett. **6** (2011) 024007 (13pp) doi:10.1088/1748-9326/6/2/024007

Detection of the timing and duration of snowmelt in the Hindu Kush-Himalaya using QuikSCAT, 2000–2008

Prajjwal K Panday[1], **Karen E Frey and Bardan Ghimire**

Graduate School of Geography, Clark University, 950 Main Street, Worcester, MA 01610, USA

E-mail: ppanday@clarku.edu

Received 22 December 2010
Accepted for publication 11 April 2011
Published 3 May 2011
Online at stacks.iop.org/ERL/6/024007

Abstract

The Hindu Kush-Himalayan (HKH) region holds the largest mass of ice in Central Asia and is highly vulnerable to global climate change, experiencing significant warming ($0.21 \pm 0.08\,^{\circ}$C/decade) over the past few decades. Accurate monitoring of the timing and duration of snowmelt across the HKH region is important, as this region is expected to experience further warming in response to increased greenhouse gas forcing. Despite the many advantages and applications of satellite-derived radar scatterometer data shown for capturing ice and snow melt dynamics at high latitudes, similar comprehensive freeze/thaw detection studies at lower latitudes (including the HKH region) are still absent from the scientific literature. A comprehensive freeze/thaw detection study is utilized on perennial snow/ice and seasonal snow cover for the first time in the Himalayan and Karakoram regions. A dynamic threshold-based method is applied to enhanced QuikSCAT Ku-band backscatter observations from 2000 to 2008 that (a) provides spatial maps of the timing of melt, freeze, and melt season duration, and (b) emphasizes regional variability in freeze/thaw dynamics. The resulting average melt durations for 2000–2008 are 161 ± 11 days (early May–mid-October) for the eastern Himalayas, 130 ± 16 days (late May–early October) for the central Himalayas, 124 ± 13 days (mid-May–mid-September) for the western Himalayas, and 124 ± 12 days (late May–late September) for the Karakoram region. The eastern Himalayan region has on average an earlier melt onset, a later freeze-up, and therefore a longer melt season ($\sim$5 weeks) relative to the central and western Himalayan and the Karakoram regions. Snowmelt dynamics exhibit regional and interannual variability with clear connections to terrain features, in particular elevation and aspect. With respect to ongoing controversies surrounding melt in the Himalayan region, this study provides an overall perspective of regional differences in melt onset, freeze-up, and melt duration that have important implications for glaciological and hydrological processes across the HKH region.

Keywords: QuikSCAT, radar, snowmelt, scatterometer, glaciers, Himalaya

1. Introduction

The Hindu Kush-Himalayan (HKH) region extends 3500 km across eight countries from central Afghanistan in the west to Myanmar in the east (Eriksson *et al* 2009, Messerli *et al* 2009) (figure 1). This region contains the largest amount of ice outside the polar regions and feeds the major South Asian river basins, including the Ganges, Indus, and Brahmaputra. Climate change impacts over the last several decades have been observed through significant air temperature warming and

[1] Author to whom any correspondence should be addressed.

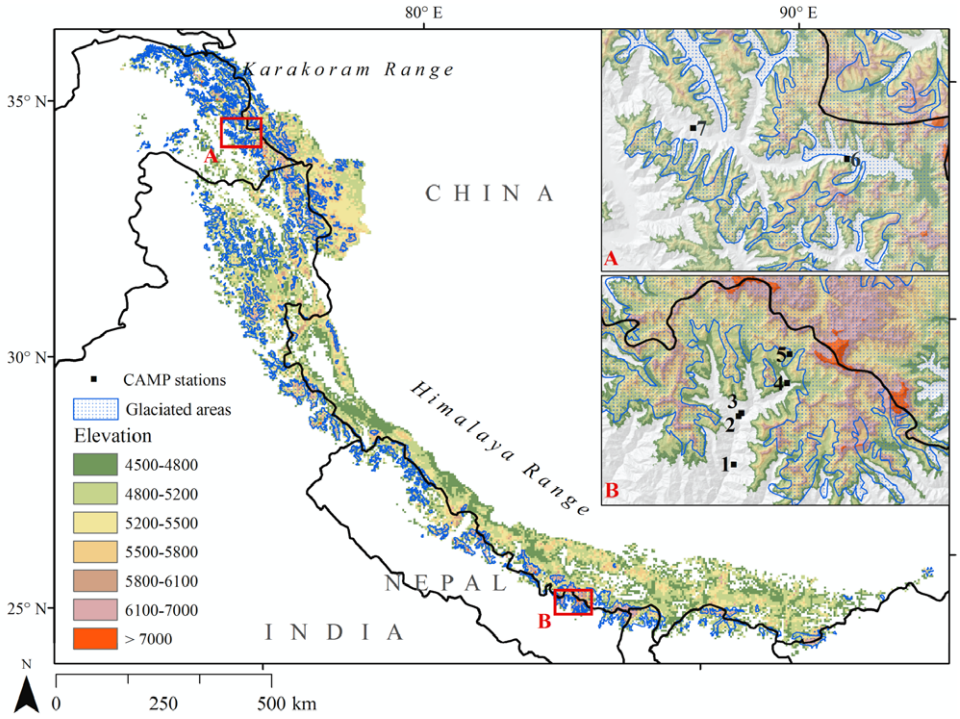

Figure 1. Study region showing glaciated areas from the Digital Chart of the World (DCW) glacier layer (Raup *et al* 2007) over the topography (>4500 m) of the Himalayan and Karakoram ranges. The inset figures show the distributions of CEOP Asia Monsoon Project (CAMP) stations in the eastern Himalaya, Nepal and Karakoram Range, Pakistan. The stations and their elevations from the elevation grid are: (1) Lukla (2543 m), (2) Namche (4043 m), (3) Syangboche (3446 m), (4) Pheriche (4589 m), (5) Pyramid (5041 m), (6) Urdukas (4395 m), and (7) Askole (3676 m).

through variable rates of retreat of glaciers across the region (UNEP 2009). For instance, recent tropospheric temperature analysis reveals widespread annual warming rates over the whole HKH region of 0.21 ± 0.08 °C/decade from 1979 to 2007 (Gautam *et al* 2009, 2010). Even greater rates have been observed for the Nepalese Himalayan region specifically, with warming at approximately 0.6 °C/decade from 1977 to 1994 (Shrestha *et al* 1999). Future climate projections indicate that the HKH region is poised for further significant warming, as the Central Asian region may experience a median temperature increase of 3.7 °C by the end of the 21st century with the greatest warming over high altitudes (particularly the Tibetan Plateau and the Himalayas) (IPCC 2007). Potential impacts of these changes will likely include substantial reductions in long-term meltwater and water supply, and further cascading effects on biodiversity and human livelihoods (Xu *et al* 2009, Immerzeel *et al* 2010). Snow and ice melt contributes significantly to the annual water supply in the HKH range, and the ability to quantify snow storage and melt accurately is therefore critical for informed management of water resources (Foster *et al* 2011).

Accurate observations of snow parameters such as snow cover extent, snow water equivalent (SWE), and timing of snow melt and refreeze across various regions are now possible due to recent advancements in optical and passive remote sensing (Foster *et al* 2011). Passive microwave sensors commonly used for snowmelt detection include the Special Sensor Microwave/Imager (SSM/I) and Advanced Microwave Scanning Radiometer (AMSR-E), where brightness temperatures (T_b) emitted from the ground increase as a result of snow melt (Bartsch *et al* 2010). Currently, global snow cover extent is available through optical sensors such as the Moderate Resolution Imaging Spectroradiometer (MODIS) (Hall *et al* 2002), while SWE is available through the AMSR-E instrument (Foster *et al* 2011). Quantification and characterization of snow parameters in the Himalayan region have focused primarily on mapping snow cover extent using optical satellite imagery (Pu and Xu 2009), and snow depth and SWE using passive microwave data (Mishra *et al* 2005). Algorithms derived from SSM/I brightness temperatures as well as field observations of SWE and snow depth have shown strong correlations and good potential for studying variability of snow cover in the Himalayas (Mishra *et al* 2005). In regions other than the Himalayas, passive microwave data (AMSR-E or SSM/I) have also been used extensively to establish the timing of the spring melt transition in the Yukon River basin (Apgar *et al* 2007), Juneau Icefield (Ramage and Isacks 2002), and across the pan-Arctic (Tedesco *et al* 2009).

In contrast to optical and passive microwave sensors, however, satellite-borne active microwave scatterometers provide an ideal tool for monitoring the seasonal transition of snow cover because of their broad spatial coverage, near-daily temporal resolution, and high sensitivity to the presence of liquid water at all weather and day/night conditions (Wismann 2000, Wang *et al* 2005). Radar scatterometers record measurements of the backscatter, expressed as the backscatter coefficient σ^0 in dB, which strongly decreases upon thawing

of frozen dry surfaces (Bartsch *et al* 2010) and has been successfully utilized to detect the timing of melt onset over major polar ice sheets and glaciers (Long and Drinkwater 1999, Wismann 2000, Smith *et al* 2003). The resulting sharp backscatter decrease upon detection of liquid water is coincident with the rise of air temperatures above 0 °C and is a well-established phenomenon over glaciers, snow, and ice (e.g., Smith *et al* 2003, Nghiem *et al* 2005, Wang *et al* 2005). The reduction in σ^0 that occurs during the melt season due to increased microwave absorption is robust enough that it can be easily used for melt mapping. For instance, radar scatterometer data have been used for identifying snow and ice melt onset and freeze dates across the pan-Arctic (Wang *et al* 2008), mapping the extent and duration of surface melt and the distribution of ice layer formation on the Greenland ice sheet (Wang *et al* 2007), estimating snow accumulation on the Greenland ice sheet (Drinkwater *et al* 2001), and determining the timing of melt onset/freeze-up on Arctic ice caps (Smith *et al* 2003, Wang *et al* 2005, Sharp and Wang 2009).

However, radar scatterometer studies of melt detection at low-latitude alpine regions are limited or non-existent. Accurate monitoring of the timing and duration of snowmelt across the Himalayan range is critical, as this region is expected to experience further warming in response to increased greenhouse gas forcing (Nogués-Bravo *et al* 2007). In this study, we examine the application of radar scatterometer data for snowmelt detection in the HKH region by applying a dynamic threshold-based algorithm to nine years (2000–2008) of enhanced resolution QuikSCAT scatterometer data, and subsequently analyze the timing of freeze/thaw events and duration of annual melt seasons. As such, our resulting time series provide a new measure of melt season variability across the entire HKH region for the last decade.

2. Data and methods

2.1. Study area

This study focuses on the Himalaya and the Karakoram mountain regions within the greater HKH region (figure 1). The Himalayan range lies at the southern edge of the Tibetan Plateau and extends from eastern Nepal, Bhutan, Sikkim and southeastern Tibet in the east to the northwestern and western Indian Himalayas in the west. The Karakoram region lies to the west of the Himalayas and is separated by the Indus River. An updated glacier inventory reports 20 182 glaciers in the Himalaya and Karakoram regions covering 43 178 km^2 (Cogley 2011). The Karakoram region consists of large, connected glacier systems with long glaciers averaging lengths of 25.4 km, while the glaciated Himalayan region (particularly in the Nepalese Himalaya) is distributed as individual glaciers with average lengths of 8.1 km (Williams and Ferrigno 2010). Despite an incomplete glacier inventory, the glacier volume for the high mountains in Central Asia is estimated to be 12 483 ± 462 km^3, derived from statistical upscaling of glacier inventory data (Radić and Hock 2010). Other regional estimates of glacier volume report 3076 km^3 in India and Pakistan, 740 km^3 in Nepal and Bhutan, and 5600 km^3 in China, the latter being the only complete glacier inventory in Central Asia (Ohmura 2009). These volumes represent a substantial fraction of the total global volume of mountain glaciers and ice caps (excluding Greenland and Antarctica), estimated to be 1.0 × 10^6 km^3 (Ohmura 2009).

The summer monsoon dominates the climate of this region and provides most of the total annual precipitation between June and September (Chalise 1994). Monsoonal precipitation decreases from east to west along the Himalayas, with average annual precipitation of ∼1071 mm in the eastern Himalaya (Brahmaputra River basin) and ∼423 mm in the western Himalaya (Indus River basin) (Immerzeel *et al* 2010). The western Himalayan and Karakoram regions are primarily influenced by westerly-dominated precipitation which brings snow and rain during winter and spring, although in some years summer-monsoon-derived precipitation is also strong enough to penetrate into the Karakoram region (Young and Hewitt 1990, Kargel *et al* 2009). A substantial portion of the annual precipitation falls as snow at altitudes above 3000 m above mean sea level, which also feeds the extensive Himalayan glaciers across the region (Eriksson *et al* 2009).

2.2. QuikSCAT enhanced resolution images

The NASA Scatterometer Climate Record Pathfinder (SCP) project has developed a radar scatterometer-based data time series to support climate studies which is publicly available (http://www.scp.byu.edu/). The SeaWinds scatterometer aboard the QuikSCAT satellite makes measurements at Ku-band (13.4 GHz) and provides 90% global backscatter coverage every 2 days with a 0.25 dB relative accuracy (Tsai *et al* 2000). Reconstruction of surface backscatter (σ^0) at finer spatial resolution using the Scatterometer Image Reconstruction (SIR) algorithm provides ascending, descending, and all-pass images in two forms termed 'egg' and 'slice' (Long and Hicks 2005). Egg-based QuikSCAT images have a nominal pixel spacing of 4.45 km and estimated effective resolution of 8–10 km, while slice-based images have a pixel spacing of 2.225 km and an effective resolution of ∼5 km (although they are noisier and more sensitive to calibration errors) (Long and Hicks 2005). The QuikSCAT σ^0 signal for snow is stronger at horizontal polarization owing to lower incidence angles than that at vertical polarization (Wang *et al* 2007). Therefore, in order to capture the maximum melt signature, enhanced resolution QuikSCAT egg-based all-pass horizontal polarization images from 2000 to 2008 were used for melt detection due to their reduced noisiness and lower sensitivity to errors. Non-polar image products, such as those used for this study, have a temporal resolution of 4 days.

Topographic data available from the SCP project were also used for analysis of melt dynamics. Digital elevation data, which are derived from the ETOPO2 global elevation dataset (a 2 min pixel resolution dataset available from the National Oceanic and Atmospheric Administration), are available in the same format, resolution, and projection as the enhanced QuikSCAT images.

2.3. In situ data from meteorological stations

The Khumbu region in the eastern Himalayas and Karakoram region in northern Pakistan are recognized as sites for the coordinated enhanced observing period (CEOP) reference sites and a network of Automated Weather Stations (AWS) has been established over a stretch of 40 km at different altitudes (Ueno *et al* 2008). Meteorological data were obtained from this network for seven stations: Pyramid (5041 m), Pheriche (4589 m), Syangboche (3446 m), Namche (4043 m) and Lukla (2543 m) in the Khumbu region, and Urdukas (4395 m) and Askole (3676 m) stations in northern Pakistan. Pyramid station is located on a ridge next to the Khumbu Glacier tongue in the Himalayan region and Urdukas station is located on the lower, southern portion of the Baltoro glacial moraine in the Karakoram region. Of the other stations, Askole station is located on a seasonally snow-covered moraine platform near the Baltoro Glacier, Pheriche station is located on bare ground with seasonal snow cover in the Khumbu Valley, and Syangboche, Lukla, and Namche stations are located on rocky, bare ground at lower elevations with seasonal snow cover in the eastern Himalaya. Available hourly temperature data between the 2000 and 2008 period were averaged into mean daily measurements. Temperature data were available from 2000 to 2004 for the Himalayan stations and from 2005 to 2007 for the Karakoram stations. The daily surface air temperature observations from these stations were then used to assist in the interpretation and calibration of the σ^0 signal as well as to evaluate the scatterometer-based observations of melt and freeze-up events. While previous studies have utilized air temperature from global reanalysis products such as the National Center for Environmental Protection–National Center for Atmospheric Research (NCEP–NCAR) to validate timing of events regionally in the Arctic (Stroeve *et al* 2006) and to correlate regional climatic controls to melt events (Sharp and Wang 2009), its applicability to topographically complex regions such as the HKH requires further analysis.

2.4. QuikSCAT backscatter melt signature algorithm

Previous studies of melt detection have developed threshold-based techniques utilizing the temporal variability of backscatter time series (Wismann 2000, Wang *et al* 2008). Other methods have utilized the significance of diurnal changes (differences between morning and evening backscatter) with respect to long-term noise to determine a QuikSCAT melt signature (Nghiem *et al* 2005, Bartsch *et al* 2007). Ashcraft and Long (2006) provide a review of comparison of different methods for melt detection over Greenland using active and passive microwave measurements. Considering the large spatial extent and complex snow conditions due to topography, we modified the melt detection algorithm used by Wang *et al* (2007) by adjusting the threshold to identify persistent melt/freeze-up events and duration of melt season for the study region.

Time series of radar backscatter values were initially extracted at AWS sites to compare with *in situ* daily air temperature data for evaluation of the robustness of a scatterometer-based melt detection algorithm. Figure 2 shows a typical backscatter time series from this region at Pyramid (27.96°N, 86.81°E), Urdukas (35.72°N, 76.29°E), Pheriche (27.89°N, 86.82°E), Askole (35.68°N, 75.82°E) and Syangboche (27.81°N, 86.72°E) stations, where the first three are the AWSs at the highest available altitudes. These meteorological stations were used to calibrate and evaluate the threshold-based algorithm as well as to determine the viability of the algorithm across an elevational gradient in the QuikSCAT dataset. Scatterometer time series show distinct seasonality, where the summer backscatter is significantly lower compared to that during winter because of increased microwave absorption within a wet snowpack (Wang *et al* 2008). The annual time series is divided into two groups (January–July and July–December), each approximately encompassing the melt onset and freeze-up events, respectively. A slightly modified threshold-based melt detection technique was therefore used to map melt onset and freeze-up (figure 3):

$$M = W_{\mathrm{mn}} - a \tag{1}$$

where W_{mn} is the mean σ^0 for February, and a is a user-defined constant. A review of the literature indicates a range of thresholds used for melt detection; for instance a 1.7 dB threshold was used in the pan-Arctic region (Wang *et al* 2008), 2.0 dB was used in Greenland (Wang *et al* 2007), and 3.5 dB was used on the Eurasian Arctic ice caps (Sharp and Wang 2009). The use of these thresholds is dictated by the reduction in backscatter profiles at the onset of melt, which generally ranges between 7 and 20 dB on polar ice caps and at higher latitudes with abundant snow cover (Wang *et al* 2007, 2008), and between 2 and 5 dB at stations with moderate forest cover and thinner snow cover (Wang *et al* 2008). In our case, the backscatter reductions that occur at melt onset across all stations in the HKH region are not nearly as drastic as those found across higher latitudes (figure 2). As such, melt onset and freeze-up were drastically underestimated for the HKH region when we applied typical thresholds (a) from previous studies (Ashcraft and Long 2006, Wang *et al* 2007, 2008, Sharp and Wang 2009) that utilized QuikSCAT for melt detection on land ice at higher latitudes and polar regions. The optimal value for a (0.58 dB) was identified empirically by comparing air temperature time series from available AWS sites with scatterometer time series at the same locations, further adjusting the value as necessary using a trial and error approach similar to Wang *et al* (2008). Through empirical evaluation of the threshold using air temperatures at AWS stations, we arrived at a threshold value that was more specifically attuned to this region. For each pixel, when σ^0 remained below M from January to July for two or more consecutive images, the image with the pixel value closest to M was identified as the timing of melt onset. Similarly, when σ^0 remained above M for two or more consecutive images between July and December, freeze-up was identified as the image closest to M plus one image. Given the four day availability of QuikSCAT data, it is impossible to detect and exclude all the refreezing events (if any occur) within the melt season. As such, although QuikSCAT-derived results can potentially overestimate melt duration (particularly at higher

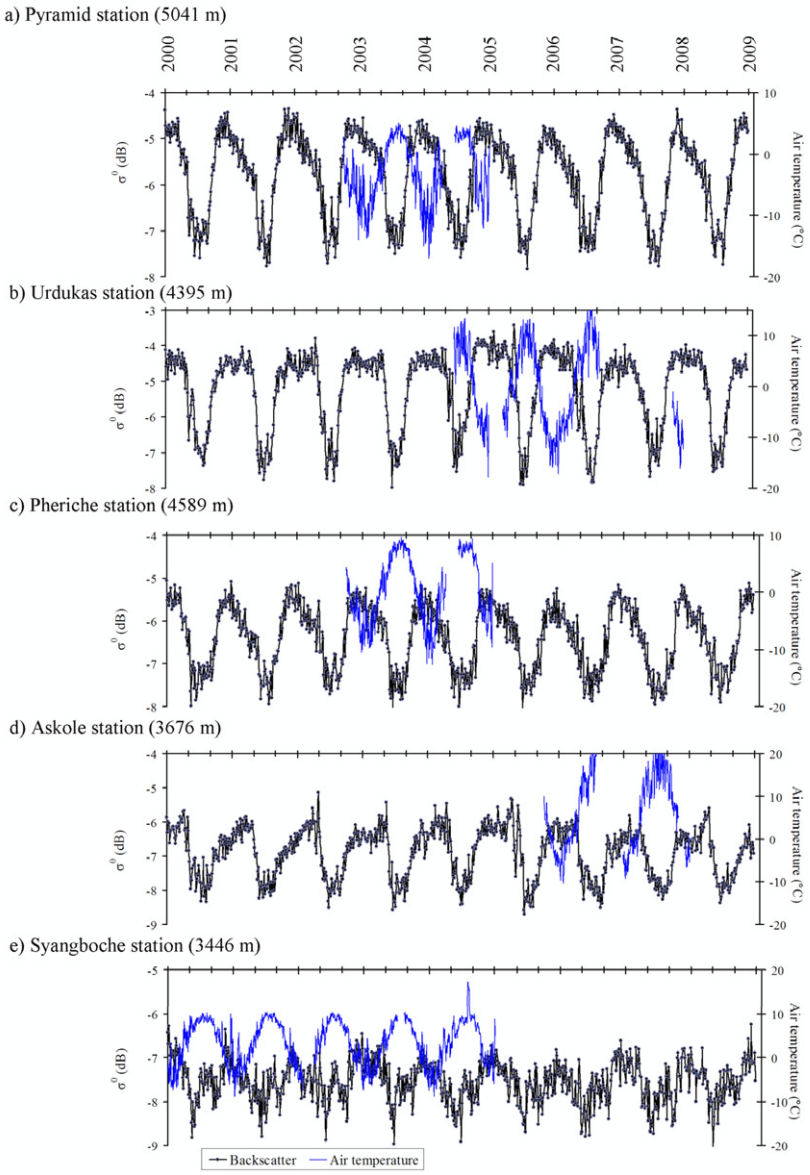

Figure 2. QuikSCAT time series of backscatter at (a) Pyramid, (b) Urdukas, (c) Pheriche, (d) Askole, and (e) Syangboche CAMP stations, plotted with available mean daily air temperature measurements.

elevations where refreezing is possible during the melt season), we focus here only on the persistent onset of melt and freeze. Once the timing of persistent melt and freeze-up events was identified, the annual melt duration was defined as the number of days between melt onset and freeze-up.

Our threshold method utilized here is applicable to pixels where the σ^0 signal exhibits a successive, distinct decrease during melt season, and therefore greatest confidence was placed on those areas with elevations >4500 m. For instance, at high elevations (>4500 m), backscatter profiles for glaciers, perennial snow cover, and seasonal snow cover showed very similar behavior and exhibited distinct drops in backscatter at the onset of melt (figures 2(a)–(d)). This regularly behaved melt signature of backscatter is generally observed down to elevations ∼3500 m (figure 2(d)), but below these elevations irregular backscatter responses are likely confounded by mixed seasonal snow/land effects (e.g., figure 2(e)). To examine melt climatology and regional variability in melt dynamics, we used 4500 m as a conservative elevation threshold to limit our analyses to the highest elevations and capture the most robust melt signatures. Annual melt onset timing, freeze-up timing, and melt duration were also mapped by applying this algorithm across the Himalaya and Karakoram regions from 2000 to 2008. The variability and anomalies of annual melt duration, melt onset timing, and freeze-up timing during the 2000–2008 period were examined across four sub-regions (eastern, central, and western Himalaya and Karakoram region).

The Himalaya and Karakoram regions are concentrated in mountain regions with high relief, which may affect the timing of melt onset and freeze-up at local scales. Therefore, snowmelt dynamics were also analyzed with respect to the spatial variability of terrain features such as elevation and

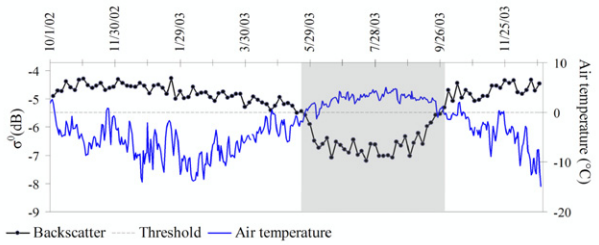

Figure 3. QuikSCAT time series of scatterometer backscatter and daily average air temperature for the 2002–2003 period at Pyramid station. The horizontal dashed line represents both the threshold ($W_{mn} - a$) used for melt onset and freeze-up detection and the 0 °C air temperature threshold, while the shaded gray area indicates the annual melt duration for that particular year.

aspect. The aspects were classified into four categories: northward facing (315 < aspect < 45), eastward facing (45 < aspect < 135), southward facing (135 < aspect < 225) and westward facing (225 < aspect < 315) slopes, while the elevations were categorized into 3500–4000, 4000–4500, 4500–5000, 5000–5500, and above 5500 m. While we take a conservative approach and focus on areas >4500 m only for most of our analyses, we have included the mid-elevation ranges (3500–4500 m) when examining melt dynamics as a function of terrain features (elevation and aspect) for simple first-order explorations of these regions that seem to behave in a predictable way when compared with air temperature data (figure 2(d)). Although our algorithm may also identify melt/freeze events in seasonally snow-covered areas (and potentially in mixed snow/land pixels) at lower elevations (<3500 m), weaker backscatter response in these regions easily misclassifies the timing of melt and freeze. Therefore, our study focuses primarily on elevations >4500 m and, while we explore melt dynamics in a limited way for elevations 3500–4500 m, we do not explore melt dynamics at all for elevations <3500 m. Finally, significant differences in timing of melt onset and freeze-up as well as melt duration were assessed individually using independent two-sample *t*-tests between all possible paired levels of grouping variables (region, elevation, and aspect).

3. Results

As surface air temperatures at the AWS sites exceed 0 °C, there are corresponding backscatter decreases consistent across the stations (figure 3). Annual melt onset, freeze-up, and melt duration maps for the 2000–2008 period (as well as their overall 9 year average) are shown in figures 4–6, respectively, for the Himalayan and Karakoram regions at elevations >4500 m. At these elevations, melt typically begins between 29 April and 11 May in the eastern Himalaya, between 14 May and 9 June in the central Himalaya, between 4 May and 30 May in the western Himalaya, and between 21 May and 4 June in the Karakoram region (figure 4). Freeze-up typically occurs between 28 September and 21 October in the eastern Himalaya, between 21 September and 11 October in the central Himalaya, between 13 September and 29 September in the western Himalaya, and between 18 September and 14 October in the Karakoram region (figure 5). In general, the eastern Himalayan region in Nepal and Bhutan shows earlier melt onset and later freeze-up dates than the central Himalayan, western Himalayan, and Karakoram regions. As a result of earlier melt onset and later freeze-up, the eastern Himalaya has on average an ∼5 week longer annual melt duration compared to the other regions for the 2000–2008 period (figure 6).

Spatial variability of the average dates of melt onset and freeze-up as well as annual melt duration for the 2000–2008 period were additionally examined as a function of elevation and aspect across the study area. The differences in timing of melt onset and freeze-up as well as duration of melt season across all elevation ranges were statistically significant at a 95% confidence interval based on independent two-sample *t*-tests. Melt onset typically begins in late March/early April at elevations of ∼4000 m and ∼15 days later (in late April/early May) at elevations of ∼5000 m (figure 7(a)). Freeze-up occurs later with decreasing elevation and is thus delayed to early October for elevations of 4500–5000 m and mid-October for elevations of 3500–4000 m (figure 7(b)). The delay in freeze-up between high elevations (>5000 m) and low elevations (3500–4000 m) is approximately 15 days. Lower elevation ranges (3500–4000 m) have an average annual melt duration of approximately 6 months, which is ∼33 days longer than the melt duration at higher elevations (4000–5000 m) and ∼53 days longer than at elevations above 5000 m (figure 7(c)). The highest elevation range (>5500 m) shows melt durations that are slightly longer than those at 5000–5500 m. This is likely an indication that high elevations (>6000 m), which occupy a small fraction (∼3%) of the overall region, may lead to the inability to reliably capture variability of snowmelt dynamics. The differences in dates of melt onset and freeze-up as well as duration of melt across different aspects were not statistically significant at the 95% confidence interval based on *t*-tests. However, at elevation ranges of 3500–5000 m, southward facing slopes have average dates of melt onset ∼4 days earlier, average dates of freeze-up ∼3 days later, and average melt duration ∼7 days longer compared to other aspects at the same elevation ranges. This departure in the dates of melt onset and freeze-up as well as duration of melt among different slope aspects disappears above 5500 m.

Nine year melt climatologies for the dates of melt onset/freeze-up and duration of melt were also examined for the four sub-regions across the HKH separately: eastern, central, and western Himalayas and the Karakoram region for areas above 4500 m elevation (figure 8(a)). The total areal percentages and mean elevations of areas above 4500 m for each region, respectively, are 37% and 5047 m for the eastern Himalaya, 41% and 5130 m for the central Himalaya, 34% and 5071 m for the western Himalaya, and 74% and 5278 m for the Karakoram region. While areas above 4500 m represent a greater proportion of the Karakoram region than for the other regions, focusing on these highest elevations across all regions allows for a more direct comparison of regional melt season dynamics. For the 2000–2008 period, the average date of melt onset is 5 May ± 5 days for the eastern Himalaya,

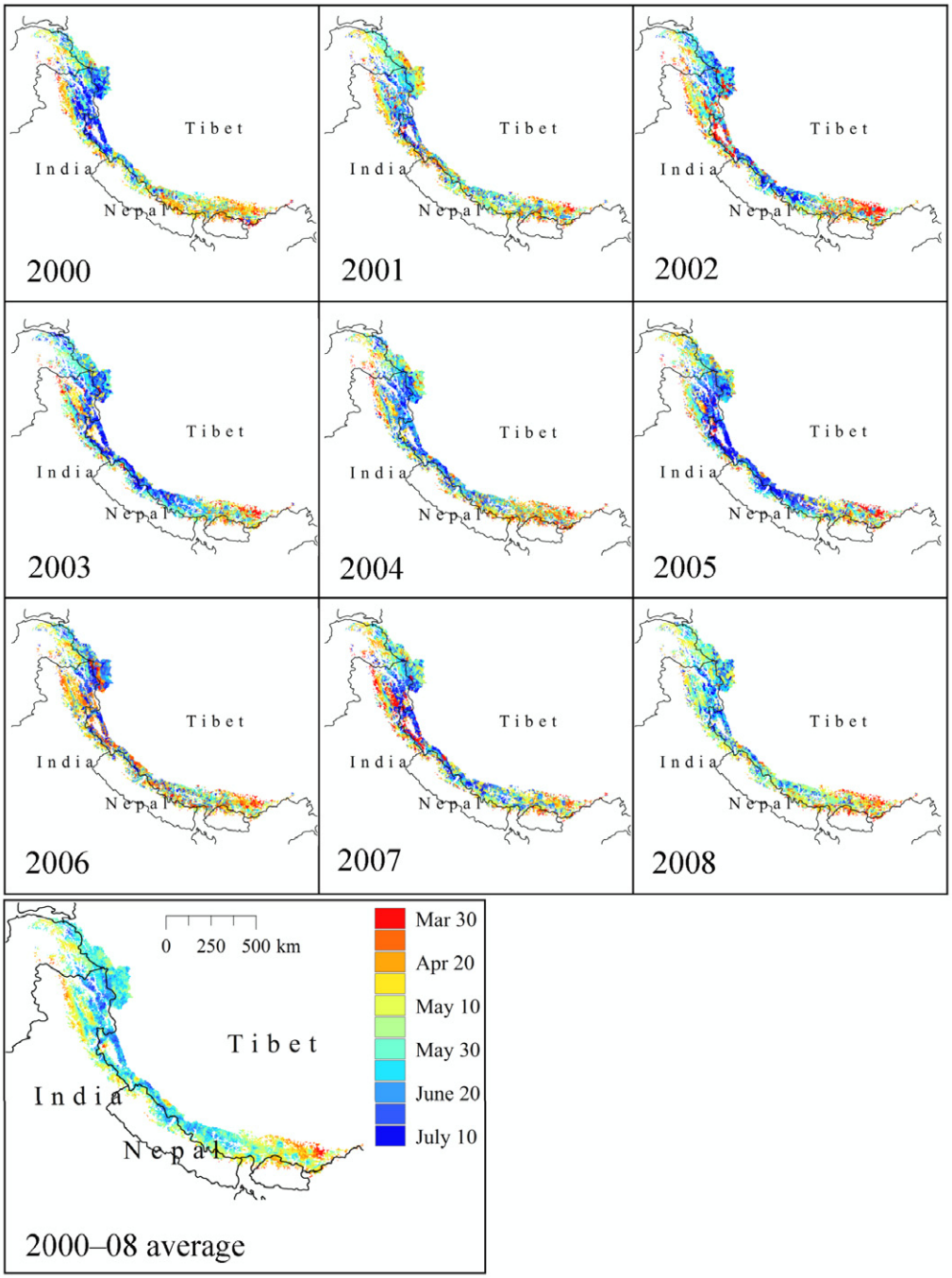

Figure 4. Annual and average melt onset dates for elevations above 4500 m for the 2000–2008 period.

26 May ± 10 days for the central Himalaya, 21 May ± 9 days for the western Himalaya, and 29 May ± 4 days for the Karakoram region (figure 8(b)). The average date of freeze-up is 14 October ± 8 days for the eastern Himalaya, 3 October ± 7 days for the central Himalaya, 23 September ± 6 days for the western Himalaya, and 2 October ± 9 days for the Karakoram region (figure 8(c)). Average melt duration is 161 ± 11 days for the eastern Himalaya, 130 ± 16 days for the central Himalaya, 124 ± 13 days for the western Himalaya, and 124 ± 12 days for the Karakoram region (figure 8(d)). The dates of melt onset and freeze-up as well as duration of melt season in the eastern Himalaya compared to the other regions were significantly different at the 95% confidence interval based on *t*-tests. The difference in melt onset between the western Himalaya and Karakoram regions was significant, and the western Himalaya also differed significantly from the central Himalaya in the timing of freeze-up based on *t*-tests. All other comparisons of regional melt characteristics were not significantly different.

Spatial averages and anomalies of melt onset, freeze-up and melt duration for individual years across the Himalayan and Karakoram regions show considerable scatter with little suggestion of trend (figure 9). Negative anomalies imply

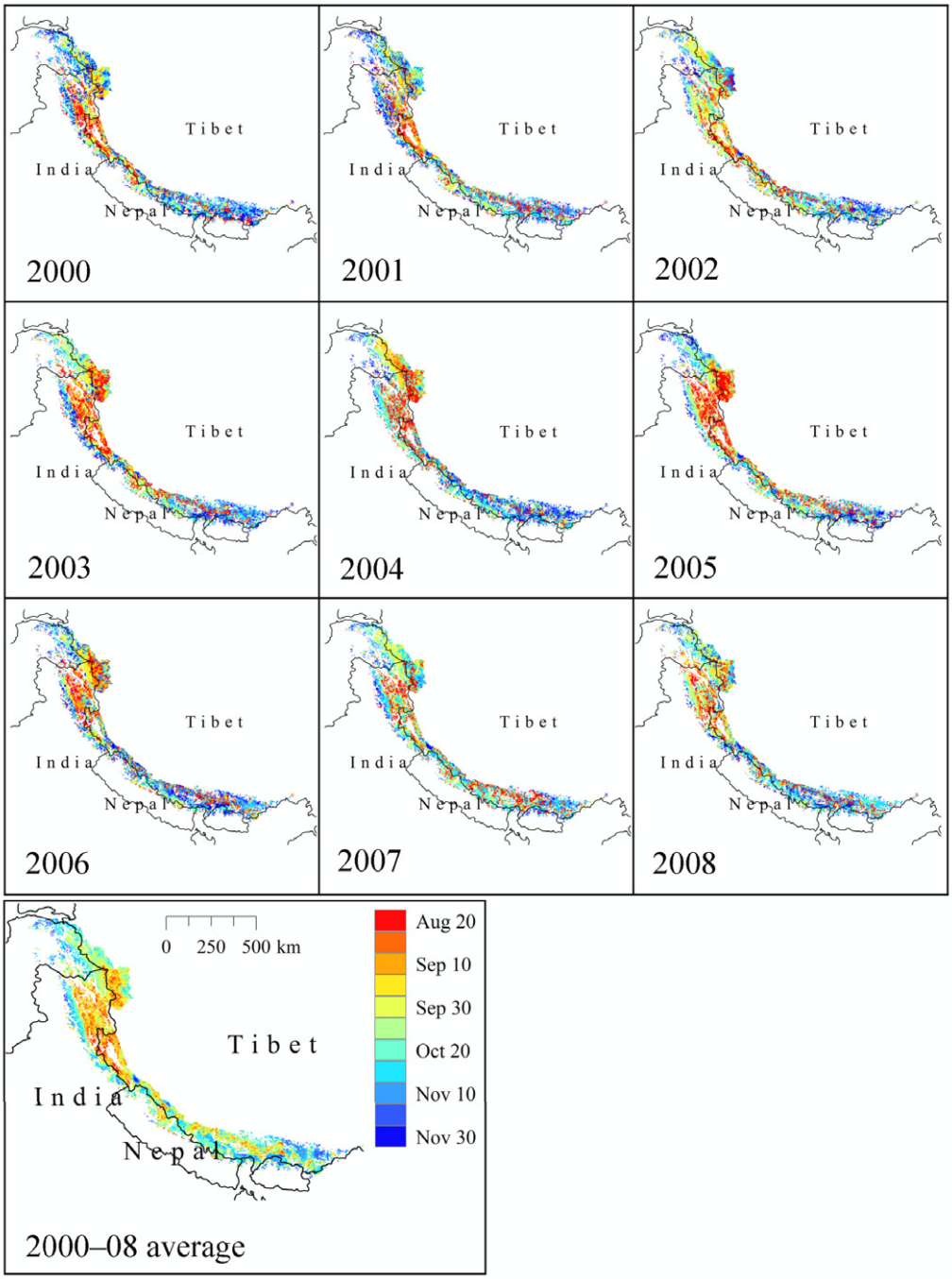

Figure 5. Annual and average freeze-up dates for elevations above 4500 m for the 2000–2008 period.

an early melt onset, early freeze-up, or shorter melt season, while positive anomalies imply a late melt onset, late freeze-up, or longer melt season. Although the eastern Himalaya compared with the other three regions is characterized by fewer large anomalies in melt dynamics for the 2000–2008 period, anomalously early freeze-up accounts for a shorter melt duration in 2007. The largest anomalies (positive or negative) in melt onset and consequently in melt duration occur in the central and western Himalaya, suggesting high interannual variability in melt compared to the other regions. Anomalously early melt onset contributed to longer melt seasons in 2002 (for the western Himalaya) and 2006 (for the central Himalaya), while late melt onset contributed to the shortening of the melt duration in 2003 (for the central Himalaya) and 2005 (for the central and western Himalayas). As a result, the central and western Himalayas exhibit greater interannual variability than the other regions due to larger melt onset anomalies (figures 9). Melt duration in the Karakoram region is primarily affected by the timing of freeze-up, with early freeze-up accounting for shorter melt seasons (2003 and 2004), and late freeze-up accounting for longer melt seasons (2000 and 2001).

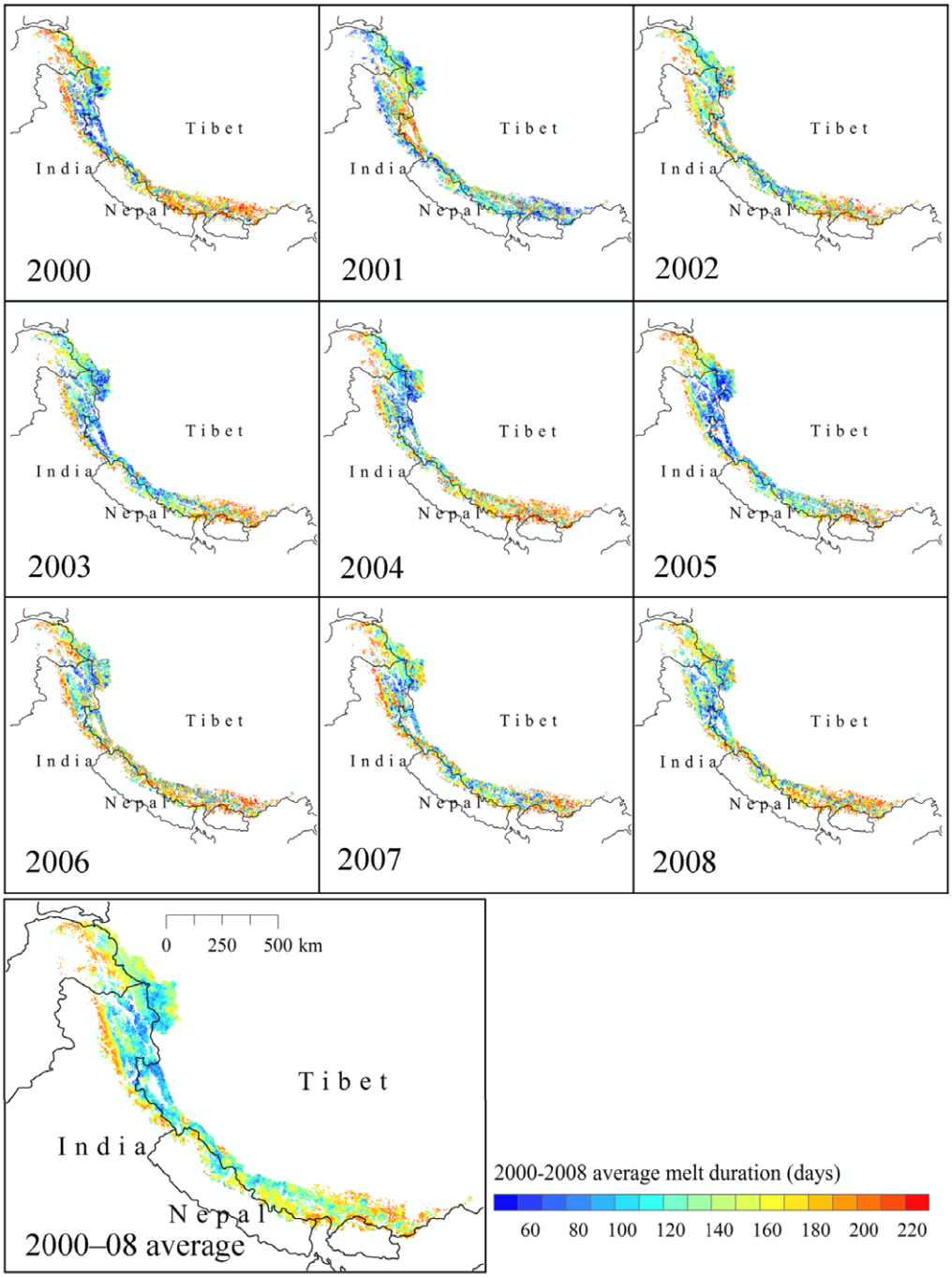

Figure 6. Annual and average melt duration for elevations above 4500 m for the 2000–2008 period.

4. Discussion and conclusions

Changes in the timing, amount, and seasonal variation of snow cover have critical implications for the glaciological and hydrological regimes of mountainous regions (Barnett *et al* 2005). Characterization of snow storage at a drainage basin scale through melt dynamics and duration provides dynamic indices for detection and monitoring of spatial and temporal hydrological changes, which is vital for improved management of water resources in this region (Foster *et al* 2011, Stewart 2009). Although both active and passive microwave measurements can be used for melt detection studies (Ashcraft and Long 2006, Bartsch *et al* 2010), our understanding of freeze/thaw phenomena through application of radar scatterometer data, particularly QuikSCAT, has improved over the last decade (Ashcraft and Long 2006, Brown *et al* 2007, Wang *et al* 2008). In contrast, the approach using passive microwaves is based on signal differences between two wavelengths and hence the assumed relationship to surface processes of freeze/thaw is unclear (Bartsch *et al* 2007). While a number of previous studies conducted in the polar regions have detected the freeze/thaw cycle utilizing

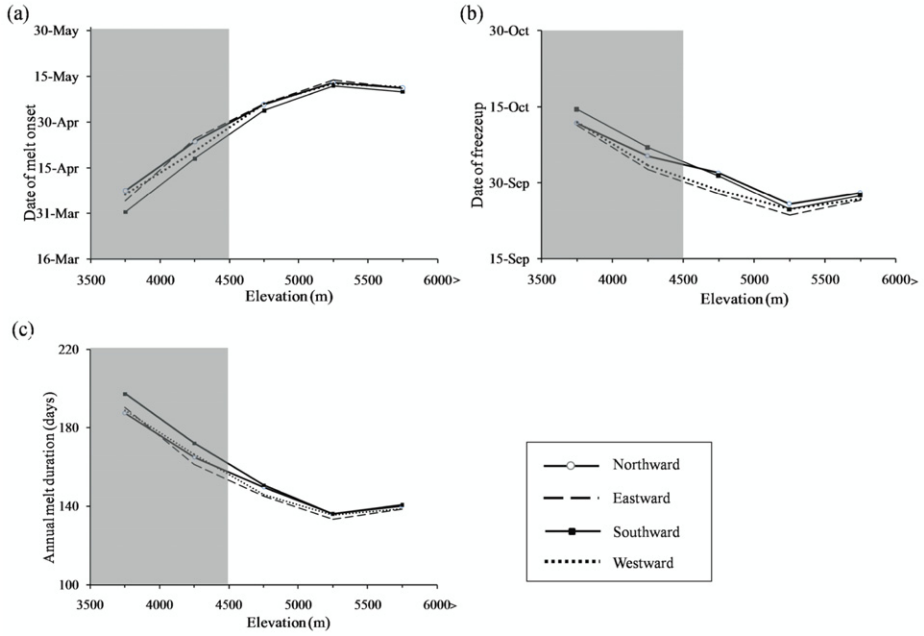

Figure 7. (a) Average melt onset, (b) average freeze-up, and (c) average melt duration for 2000–2008 as a function of elevation for different slope aspects. While there is strong evidence of melt signatures at the 3500–4500 m elevation range (figure 2(c)), a conservative approach is taken and greatest confidence is placed on melt statistics derived at elevations above 4500 m (where the most robust melt signatures are found (figures 2(a) and (b))). Melt dynamics for the 3500–4500 m range (gray regions) are shown to provide first-order observations of melt dynamics as a function of terrain characteristics.

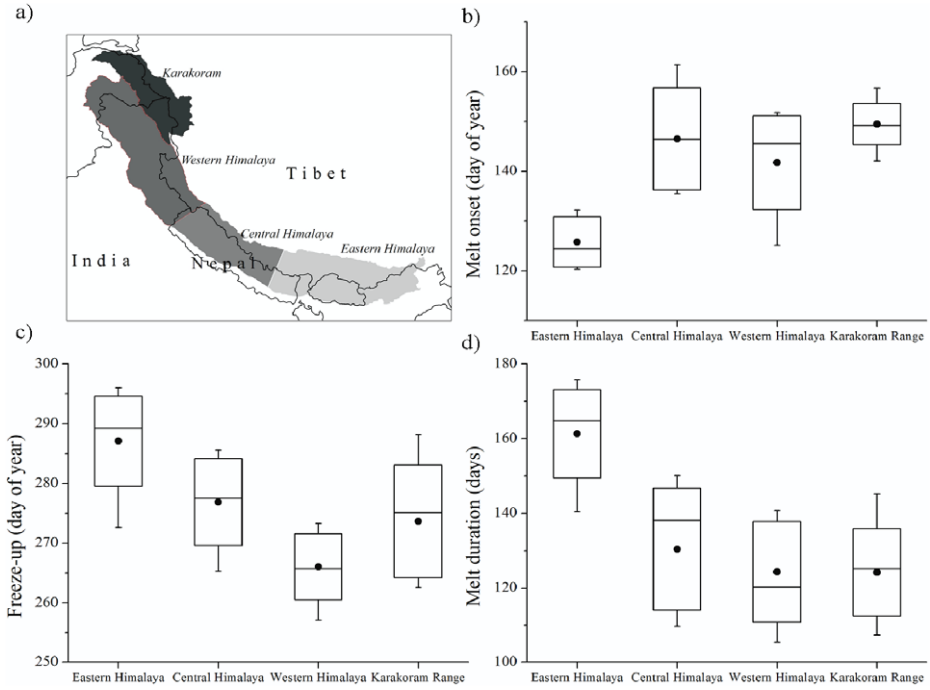

Figure 8. (a) Zonation of the eastern, central, and western Himalaya and the Karakoram range, and simplified box plots of (b) melt onset, (c) freeze-up and (d) melt duration for the years 2000–2008 for each region for elevations above 4500 m. In each box plot, the box represents a ± 1 standard deviation from the mean (black dot) and the line inside the box denotes the median. The whiskers in the plots represent the minimum and maximum values for each distribution.

scatterometer data, this is currently the only known study that uses scatterometer data to detect melt onset/freeze-up across the HKH region. This study has indeed shown that the backscatter level for pre-melt conditions provides a reference that sufficiently contrasts with backscatter response during melt events in the HKH region, similar to that observed at higher latitudes. In doing so, we present a first comprehensive freeze/thaw detection study for the HKH

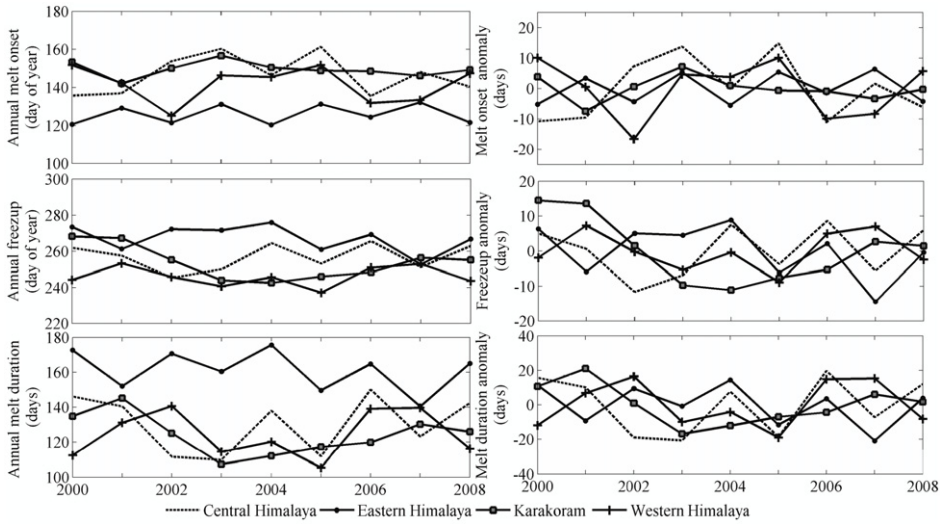

Figure 9. Melt climatologies showing averages and anomalies of annual melt onset, freeze-up and melt duration for elevations above 4500 m across the four regions in this study, for 2000–2008.

region that (a) provides spatial maps of the timing of melt onset/freeze-up, and duration of annual melt season, and (b) emphasizes regional variability in melt onset, freeze-up and melt duration for the last decade.

Previous studies of melt detection in this region have either focused mostly on the Tibetan Plateau utilizing optical satellite imagery (Pu and Xu 2009) or only explored the capability of multi-sensor satellite data to derive a global snowmelt product at a coarse resolution (∼25 km) (Foster *et al* 2011). To our knowledge, this is the first study to investigate the application of radar scatterometer data for freeze/thaw detection at a finer resolution (∼5 km) in the HKH region specifically. Although our study excludes the Tibetan Plateau from our analyses, there are several similarities that can be drawn between these studies. Both studies report a clear linkage with terrain features (in particular elevation), with the MODIS-derived onset of snow ablation occurring at the end of February at lower elevations and delayed until mid-March at 3000 m, April at 4000 m, and May at elevations above 5000 m. Our study places highest confidence in melt detection at elevations above 4500 m. Although we are less certain that the detected melt onset and freeze-up are associated with the most persistent seasonal melt events for the mid-elevation ranges (3500–4500 m), melt onset derived for these elevation ranges compared well with those derived from MODIS snow cover.

Pu and Xu (2009) also reported large interannual variability and hence large anomalies of snow cover from the climatological mean (2000–2006) during late fall and winter months. At higher latitudes, deep snow cover is associated with relatively long melt duration, while shallow snow cover is associated with short melt duration (Wang *et al* 2008). Similar phenomena at lower latitudes may explain the anomalies in melt onset and freeze-up as observed in this study. The western Himalaya and Karakoram regions are influenced by the westerly-dominated precipitation, which brings a majority of the snowfall during winter in this region. Therefore regional variability in precipitation will contribute to variability in melt duration in these regions. Another study using the Indian National Satellite (a high-resolution radiometer) derived snow cover estimates for the 1986–2000 period over the western Himalayan region has indicated an earlier snowmelt from winter to spring after 1993 (Kripalani *et al* 2003). The time period of QuikSCAT data used in this study will unfortunately remain too short for trend analysis due to the end of data collection in 2009 because of an antenna rotation failure. Although the nine years of available QuikSCAT data may be too short for any conclusive trends in snowmelt dynamics, the data may indeed lend great insight into the interannual variability across these critical regions.

We show that the eastern Himalayas experience a longer melt season compared to other regions along the HKH, which is likely due to the earlier onset of snowmelt owing to greater radiation intensity at lower latitudes compared to higher latitudes (Abdalati and Steffen 1997). The advancement and northward migration of snowmelt over the season is observed with later melt onset dates in the central Himalaya, western Himalaya, and Karakoram ranges, respectively. The findings in this study may corroborate the variable responses of glaciers from the east to the northwest, with more melting and faster glacial retreat in the eastern Himalaya, yet a lack of any rapid disintegration of glaciers in the northwestern Himalayan and Karakoram regions (Kargel *et al* 2009). As the eastern Himalayas have a longer melt season on average, enhanced melting may amplify the already observed glacial retreat (Fujita *et al* 2006, Bolch *et al* 2008, Kayastha and Harrison 2008), (Kargel *et al* 2009). In contrast, the Karakoram region may be less influenced given the shorter duration of melt and larger glaciers (Williams and Ferrigno 2010); however, accelerating rates of mass loss in northwestern glaciers as detected by the GRACE satellite from 2003 to 2009 raise concern for these regions as well (Matsuo and Heki 2010). Furthermore, timing of snowmelt dynamics may also provide useful information for ongoing studies that suggest linkages between snow cover in the Himalaya and adjacent Tibetan

Plateau and the monsoon (Kripalani *et al* 2003, Immerzeel *et al* 2009, Pu and Xu 2009). Snow cover in these regions is believed to affect the monsoonal temperature gradient from the Indian Ocean to the Himalaya and Tibetan Plateau, as a substantial fraction of solar radiation is utilized for the melting of snow (UNEP 2009). Therefore, a smaller snow cover extent and faster snow melt from winter to spring favors an early onset of monsoon, while greater snow extent delays the onset of monsoon. If annual melt duration, as derived in this study, is either anomalously short or long, it implies strong or weak monsoonal activity over India (Kripalani *et al* 2003). Therefore, an assessment of the spatial heterogeneity in climatic variability and snow melt/freeze-up will be critical when evaluating and attributing impacts of climate change, particularly in hydrological as well as glaciological studies across the HKH region.

In conclusion, we have developed a dynamic threshold-based melt detection algorithm calibrated with *in situ* air temperature records to identify melt and freeze-up events from enhanced resolution data from time series of QuikSCAT radar scatterometer data. Maps of the timing of melt onset and freeze-up as well as the annual duration of melt were also produced for the first time for the HKH ranges, which provide a comprehensive representation of snowmelt dynamics for the 2000–2008 period. These allow differentiation of spatial patterns in melt climatology and identification of the nature and magnitude of interannual variability across four sub-regions of the HKH ranges. On average, a longer melt season is observed in the eastern Himalayan region compared to the other regions of the HKH ranges by ∼5 weeks. Annual snowmelt begins first in the eastern Himalaya and progresses northwesterly, with snow in the Karakoram region melting last. On average, annual freeze-up begins first in the western Himalaya and last in the eastern Himalaya region. The eastern Himalaya is also characterized by low interannual variability in snow melt onset, freeze-up, and duration, while the central and western Himalayan regions are characterized by high interannual variability in melt onset and melt duration (but less so with freeze-up). By contrast, interannual variability in melt duration in the Karakoram region is much more driven by variability in the timing of freeze-up. The effects of complex terrain leading to heterogeneous melt processes are also likely causes of regional variability in melt onset, freeze-up, and melt duration over these mountainous regions (Wang *et al* 2008). Melt onset typically begins in late March/early April at elevations of ∼4000 m and is delayed by approximately one month at higher elevations (>5500 m). Freeze-up begins at the highest elevations (>5500 m) around late September and occurs later with decreasing elevation, with lower elevations (3500–4000 m) experiencing freeze-up around mid-October. Southward facing slopes tend to have earlier melt onset, later freeze-up, and longer annual melt duration, particularly at lower elevations, due to warmer and drier conditions from higher solar radiation inputs (Turner *et al* 2001). This study presents a first application of melt detection techniques using time series of radar scatterometer data in low latitudinal alpine regions. Amid controversies surrounding snow/glacier melt in the HKH region (Bagla 2009, Cogley *et al* 2010, Schiermeier 2010), this scatterometer-based melt detection study provides important insight into the seasonal and interannual melt dynamics of snow and ice cover, which has important consequences for hydrological processes as well as glacier mass balance across the Himalayan and Karakoram regions.

Acknowledgments

We would like to thank the following data providers: NASA Scatterometer Climate Record Pathfinder Project for the enhanced resolution QuikSCAT data, and the Ev-K^2-CNR project which maintains the CEOP Reference Sites in Nepal (CAMP/Himalayas) and in Pakistan (CAMP/Karakoram) as part of the Stations at High Altitude for Research on the Environment (SHARE) project. We would also like to thank David Long for assistance with the QuikSCAT data and J Graham Cogley for providing outline shapefiles for the Himalayan and Karakoram regions. This research was funded in part by a NASA Earth System Science Fellowship (Grant No. NNX10AO65H).

References

Abdalati W and Steffen K 1997 Snowmelt on the Greenland ice sheet as derived from passive microwave satellite data *J. Climatol.* **10** 165–75

Apgar J D, Ramage J M, McKenney R A and Maltais P 2007 AMSR-E algorithm for snowmelt onset detection in sub-arctic heterogeneous terrain *Hydrol. Process.* **21** 1587–96

Ashcraft I S and Long D G 2006 Comparison of methods for melt detection over Greenland using active and passive microwave measurements *Int. J. Remote Sens.* **27** 2469–88

Bagla P 2009 No sign yet of Himalayan meltdown, Indian report finds *Science* **326** 924

Barnett T P, Adam J C and Lettenmaier D P 2005 Potential impacts of a warming climate on water availability in snow-dominated regions *Nature* **438** 303–9

Bartsch A, Kidd R A, Wagner W and Bartalis Z 2007 Temporal and spatial variability of the beginning and end of daily spring freeze/thaw cycles derived from scatterometer data *Remote Sens. Environ.* **106** 360–74

Bartsch A, Wagner W and Kidd R 2010 *Environmental Change in Siberia: Earth Observation, Field Studies and Modelling, Advances in Global Change Research* ed H Balzter (Dordrecht: Springer)

Bolch T, Buchroithner M F, Pieczonka T and Kunert A 2008 Planimetric and volumetric glacier changes in the Khumbu Himalaya since 1962 using Corona, Landsat TM and ASTER data *J. Glaciol.* **54** 592–600

Brown R, Derksen C and Wang L 2007 Assessment of spring snow cover duration variability over northern Canada from satellite datasets *Remote Sens. Environ.* **11** 367–81

Chalise S 1994 *Mountain Environments in Changing Climates* ed M Beniston (London: Routledge)

Cogley J G 2011 Present and future states of Himalaya and Karakoram glaciers *Ann. Glaciol.* (submitted)

Cogley J G, Kargel J S, Kaser G and Van der Veen C J 2010 Tracking the source of glacier misinformation *Science* **327** 522

Drinkwater M, Long D and Bingham A 2001 Greenland snow accumulation estimates from satellite radar scatterometer data *J. Geophys. Res.* **106** JD900107

Eriksson M, Jianchu X, Shrestha A B, Vaidya R A, Nepal S and Sandström K 2009 *The Changing Himalayas: Impact of*

Climate Change on Water Resources and Livelihoods in the Greater Himalayas (Kathmandu: ICIMOD)
Foster J L, Hall D K, Eylander J B, Riggs G A, Nghiem S V, Tedesco M, Kim E, Montesano P M, Kelly R E J, Casey K A and Choudhury B 2011 A blended global snow product using visible, passive microwave and scatterometer satellite data *Int. J. Remote Sens.* **32** 1371–95
Fujita K, Thompson L G, Ageta Y, Yasunari T, Kajikawa Y, Sakai A and Takeuchi N 2006 Thirty-year history of glacier melting in the Nepal Himalayas *J. Geophys. Res.* **111** 1–6
Gautam R, Hsu N, Lau K M, Tsay S C and Kafatos M 2009 Enhanced pre-monsoon warming over the Himalayan–Gangetic region from 1979 to 2007 *Geophys. Res. Lett.* **36** L07704
Gautam R, Hsu N C and Lau K-M 2010 Pre-monsoon aerosol characterization and radiative effects over the Indo-Gangetic plains: implications for regional climate warming *J. Geophys. Res.* **115** D17208
Hall D K, Riggs G A, Salomonson V V, DiGirolamo N E and Bayr K J 2002 MODIS snow-cover products *Remote Sens. Environ.* **83** 181–94
Immerzeel W W, Beek L P H v and Bierkens M F P 2010 Climate change will affect the Asian water towers *Science* **328** 1382–5
Immerzeel W W, Droogers P, Jong S M d and Bierkens M F P 2009 Large-scale monitoring of snow cover and runoff simulation in Himalayan river basins using remote sensing *Remote Sens. Environ.* **113** 40–9
IPCC 2007 *Climate Change 2007: Synthesis Report* ed Core Writing Team, R K Pachauri and A Reisinger (Geneva: IPCC)
Kargel J *et al* 2009 *Satellite-Era Glacier Changes in High Asia* (San Francisco, CA: American Geophysical Union)
Kayastha R B and Harrison S P 2008 Changes of the equilibrium-line altitude since the Little Ice Age in the Nepalese Himalaya *Ann. Glaciol.* **48** 93–9
Kripalani R H, Kulkarni A and Sabade S S 2003 Western Himalayan snow cover and Indian monsoon rainfall: a re-examination with INSAT and NCEP/NCAR data *Theor. Appl. Climatol.* **74** 1–18
Long D G and Drinkwater M R 1999 Cryosphere applications of NSCAT data *IEEE Trans. Geosci. Remote Sens.* **37** 1671–84
Long D G and Hicks B R 2005 *Standard BYU QuikSCAT/SeaWinds Land/Ice Image Products, Report* (Provo, UT: Brigham Young University)
Matsuo K and Heki K 2010 Time-variable ice loss in Asian high mountains from satellite gravimetry *Earth Planet. Sci. Lett.* **290** 30–6
Messerli B, Viviroli D and Weingartner R 2009 *Mountains, Valleys and Flood Plains: Managing Water Resources in a Time of Global Change* ed A Garrido and A Dinar (London: Routledge)
Mishra V D, Mathur P and Singh R P 2005 Qualitative and quantitative analysis of snow parameters using passive microwave remote sensing *J. Indian Soc. Remote Sens.* **33** 381–93
Nghiem S V, Steffen K, Neumann G and Huff R 2005 Mapping of ice layer extent and snow accumulation in the percolation zone of the Greenland ice sheet *J. Geophys. Res.* **110** 1–13
Nogués-Bravo D, Araujo M B, Errea M P and Martinez-Rica J P 2007 Exposure of global mountain systems to climate warming during the 21st century *Glob. Environ. Change* **17** 420–8
Ohmura A 2009 Completing the world glacier inventory *Ann. Glaciol.* **50** 144–8
Pu Z and Xu L 2009 MODIS/Terra observed snow cover over the Tibet Plateau: distribution, variation and possible connection with the East Asian summer monsoon (EASM) *Theor. Appl. Climatol.* **97** 265–78
Radić V and Hock R 2010 Regional and global volumes of glaciers derived from statistical upscaling of glacier inventory data *J. Geophys. Res.* **115** F01010
Ramage J M and Isacks B L 2002 Determination of melt-onset and refreeze timing on southeast Alaskan icefields using SSM/I diurnal amplitude variations *Ann. Glaciol.* **34** 391–8
Raup B, Racoviteanu A, Khalsa S J S, Helm C, Armstrong R and Arnaud Y 2007 The GLIMS geospatial glacier database: a new tool for studying glacier change *Glob. Planet. Change* **56** 101–10
Schiermeier Q 2010 Glacier estimate is on thin ice *Nature* **463** 276
Sharp M and Wang L 2009 A five-year record of summer melt on Eurasian Arctic ice caps *J. Climatol.* **22** 133–45
Shrestha A B, Wake C, Mayewski P A and Dibb J E 1999 Maximum temperature trends in the Himalaya and its vicinity: an analysis based on temperature records from Nepal for the period 1971–1994 *J. Climatol.* **12** 2775–86
Smith L C, Sheng Y, Forster R R, Steffen K, Frey K E and Alsdorf D E 2003 Melting of small Arctic ice caps observed from ERS scatterometer time series *Geophys. Res. Lett.* **30** 2034
Stewart I T 2009 Changes in snowpack and snowmelt runoff for key mountain regions *Hydrol. Process.* **23** 78–94
Stroeve J, Markus T, Meier W N and Miller J 2006 Recent changes in the Arctic melt season *Ann. Glaciol.* **44** 367–74
Tedesco M, Brodzik M, Armstrong R, Savoie M and Ramage J M 2009 Pan arctic terrestrial snowmelt trends (1979–2008) from spaceborne passive microwave data and correlation with Arctic Oscillation *Geophys. Res. Lett.* **36** L21402
Tsai W-Y, Nghiem S V, Huddleston J N, Spencer M W, Stiles B W and West R D 2000 Polarimetric scatterometry: a promising technique for improving ocean surface wind measurements *IEEE Trans. Geosci. Remote Sens.* **38** 1903–21
Turner M G, Gardner R H and O'Neill R V 2001 *Landscape Ecology in Theory and Practice: Pattern and Process* (New York: Springer)
Ueno K, Toyotsu K, Bertolani L and Tartari G 2008 Stepwise onset of monsoon weather observed in the Nepal Himalaya *Mon. Weather Rev.* **136** 2507–22
UNEP 2009 *Recent Trends in Melting Glaciers, Tropospheric Temperatures Over the Himalayas and Summer Monsoon Rainfall Over India* (Nairobi: United Nations Environment Programme)
Wang L, Derksen C and Brown R 2008 Detection of pan-Arctic terrestrial snowmelt from QuikSCAT, 2000–2005 *Remote Sens. Environ.* **112** 3794–805
Wang L, Sharp M, Rivard B and Steffen K 2007 Melt season duration and ice layer formation on the Greenland ice sheet, 2000–2004 *J. Geophys. Res.* **112** F04013
Wang L, Sharp M J, Rivard B, Marshall S and Burgess D 2005 Melt season duration on Canadian Arctic ice caps, 2000–2004 *Geophys. Res. Lett.* **32** L19502
Williams R S and Ferrigno J G (ed) 2010 Glaciers of Asia *US Geological Survey* p 349
Wismann V 2000 Monitoring of seasonal snowmelt on Greenland with ERS scatterometer data *IEEE Trans. Geosci. Remote Sens.* **38** 1821–6
Xu J, Grumbine E, Shrestha A, Eriksson M, Yang X, Wang Y and Wilkes A 2009 The melting Himalayas: cascading effects of climate change on water, biodiversity, and livelihoods *Conserv. Biol.* **23** 520–30
Young G J and Hewitt K 1990 Hydrology research in the upper Indus basin, Karakoram Himalaya, Pakistan *Hydrology of Mountainous Areas* (Czechoslovakia: IASH)